Tuning and Identification of Interband Transitions in Monolayer and Bilayer Molybdenum Disulfide Using Hydrostatic Pressure

Xiuming Dou, Kun Ding, Desheng Jiang, and Baoquan Sun*

State Key Laboratory of Superlattices and Microstructures, Institute of Semiconductors, Chinese Academy of Sciences, P.O. Box 912, Beijing 100083, China

ABSTRACT Few-layer molybdenum disulfide (MoS_2) is advantageous for application in next-generation electronic and optoelectronic devices. For monolayer MoS_2, it has been established that both the conduction band minimum (CBM) and the valence band maximum (VBM) occur at the K point in the Brillouin zone. For bilayer MoS_2, it is known that the VBM occurs at the Γ point. However, whether the K valley or the Λ valley forms the CBM and the energy difference between them remain disputable. Theoretical calculations have not provided a conclusive answer. In this paper, we demonstrate that a direct K−K to an indirect Λ−K interband transition in bilayer MoS_2 can be optically detected by tuning the hydrostatic pressure. A changeover of the CBM from the K valley to the Λ valley is observed to occur under a pressure of approximately 1.5 GPa. The experimental results clearly indicate that the K valley forms the CBM under zero strain, while the Λ valley is approximately 89 $\pm$ 9 meV higher in energy.

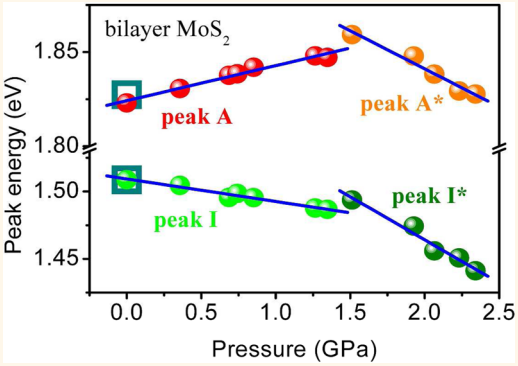

KEYWORDS: MoS_2 · hydrostatic pressure · photoluminescence · interband transition · conduction band minimum

Recently, few-layer molybdenum disulfide (MoS_2), along with other few-layer transition metal dichalcogenides (TMDs), such as $MoSe_2$, WS_2, and WSe_2, have garnered significant interest based on their unique structural, optical, and optoelectronic properties.[1−12] Monolayer MoS_2 is composed of a single layer of the transition metal molybdenum (Mo) and two layers of chalcogen (S) and thus forms what is known as a S−Mo−S sandwiched structure, wherein strong covalent bonds exist between the layers. The structures of few-layer and bulk MoS_2 are constituted by stacking MoS_2 monolayers, and a weak van der Waals force exists between these sandwiched layers. Numerous theoretical studies have discussed the influence of strain on band structure and the carrier effective mass of few-layer MoS_2 and other semiconducting TMDs.[13−34] Notable physical effects such as strain-induced direct-to-indirect band gap transition and semiconductor-to-metal transition have been predicted.[16,18,28,32,33] By applying uniaxial tensile strain (in-plane) experimentally, the direct interband transitions of monolayer and bilayer MoS_2 normally show red shifts.[35−37] Additionally, trilayer MoS_2 shows a blue shift when an in-plane compressive biaxial strain is applied.[38] Semiconductor-to-metal transition in multilayer MoS_2 has been observed by applying hydrostatic pressure.[39] The evolution of the band structure as a function of temperature has been studied for the purpose of identifying the conduction band minimum (CBM) in the Brillouin zone for bilayer MoS_2.[40] Theoretical calculations related to the energy position of the CBM of bilayer MoS_2 yield contrary results: some calculations suggest that the CBM occurs at the K point,[18,19,26,27,32] whereas others claim that it occurs at the Λ point.[2,23,25,29] However, experimental evidence for the relative energy of the K and the Λ valleys is lacking, though it is of fundamental importance. The diamond anvil cell (DAC) used as a high hydrostatic pressure device has been widely employed to study metal−semiconductor transitions, electronic

* Address correspondence to bqsun@semi.ac.cn.

Received for review May 19, 2014 and accepted July 2, 2014.

Published online July 02, 2014
10.1021/nn502717d

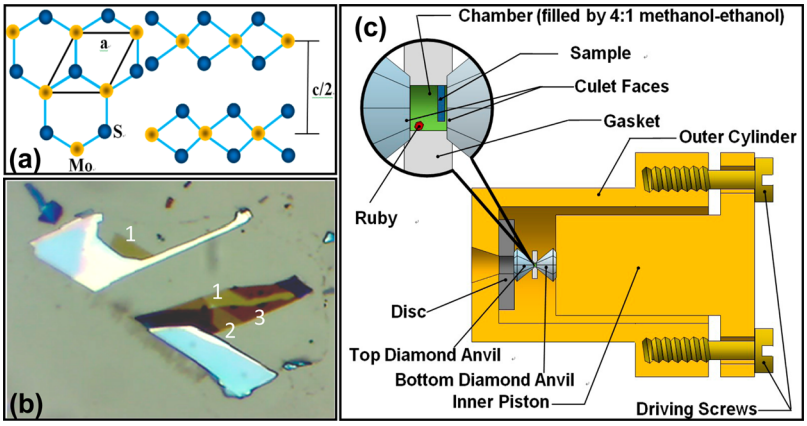

Figure 1. (a) Schematic diagrams of the lattice structure of MoS_2 in both in-plane (left) and out-of-plane (right) directions, where "*a*" and "*c*" represent in-plane and out-of-plane lattice constants, respectively. "Mo" and "S" represent the molybdenum and the chalcogen atoms, respectively. (b) Optical microscopic image of the micromechanically exfoliated MoS_2 sample. The regions labeled "1", "2", and "3" represent one-, two-, and three-layer MoS_2, respectively, identified by the optical contrast. (c) Schematic drawing of the DAC device in a cross-sectional view. The enlarged part shows the few-layer MoS_2 sample and the ruby in the DAC chamber.

structures, and optical transitions in bulk crystals and nanostructures.[41−44] It should also facilitate a powerful technique for tuning the electronic band structure and precisely identifying the optical interband transitions related to conduction band valleys and valence band hills in few-layer MoS_2.

In this article, we report a systematic experimental study on the optical gap evolutions of both monolayer and bilayer MoS_2 as increasing hydrostatic pressure up to 4.87 and 2.34 GPa for monolayer and bilayer MoS_2, respectively, using the DAC device. The pressure-dependent measurements of the photoluminescence (PL) spectra at room temperature are used to characterize their electronic band structures. With rising pressure, for monolayer MoS_2, the PL peak related to the direct interband transition undergoes a blue shift at a rate of approximately 20 meV/GPa. For bilayer MoS_2, a direct K−K to an indirect Λ−K interband transition is observed at a pressure of approximately 1.5 GPa. It is also found that the CBM occurs at the K point and that the energy difference between the K and the Λ valleys is approximately 89 ± 9 meV under ambient pressure. For the indirect interband transition, the PL peak shows a red shift under increasing pressure, and the PL emission changes from a K−Γ to a Λ−Γ interband transition at a pressure of approximately 1.5 GPa.

RESULTS AND DISCUSSION

Figure 1a shows the schematic diagrams of the lattice structure in both in-plane (left side) and out-of-plane (right side) directions for MoS_2, where *a* and *c* represent in-plane and out-of-plane lattice constants, respectively, and Mo and S represent the molybdenum and the chalcogen atoms, respectively. The monolayer and few-layer MoS_2 samples measuring a few micrometers were prepared by micromechanical exfoliation of a natural bulk MoS_2 (SPI Supplies) on a thinned SiO_2/Si substrate. Regions of one-, two-, and three-layer

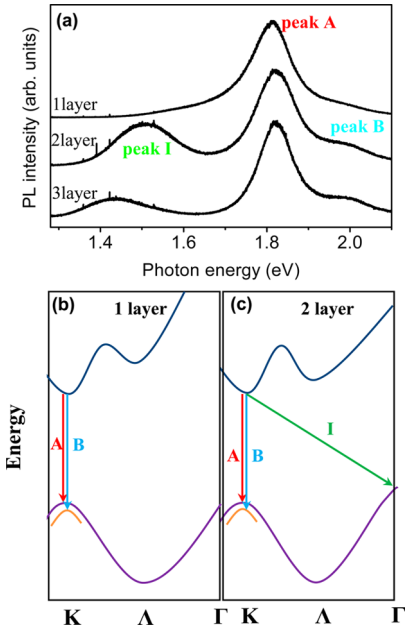

Figure 2. (a) PL spectra of one-, two-, and three-layer MoS_2 samples. Each plot is normalized based on its maximum intensity. PL peaks A, B, and I are indicated. (b,c) Schematic diagrams show the energy band structures for monolayer and bilayer MoS_2 under zero strain, where the K, Λ, and Γ points in the Brillouin zone and the interband transitions of peaks A, B, and I are identified.

MoS_2 were identified by their optical contrast with an optical microscope (Figure 1b) and further confirmed using PL measurements (Figure 2a). Micro-PL was collected at room temperature using an optical confocal microscopy setup (see Supporting Information). The pressure-dependent PL measurements were performed using a DAC device, as schematically shown in Figure 1c (details of the DAC device are in Supporting Information).

PL spectra of the monolayer, bilayer, and trilayer MoS_2 under zero strain are shown in Figure 2a. For

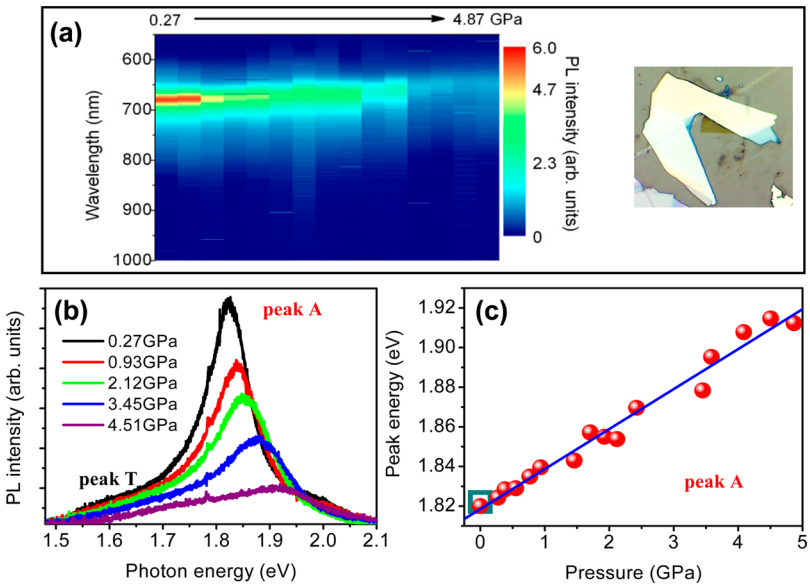

Figure 3. (a) PL intensity mapping as a function of hydrostatic pressure from 0.27 to 4.87 GPa for the monolayer MoS_2 sample, whose microscopic image is shown in the right inset. A 4:1 methanol−ethanol pressure-transmitting medium is used. (b) PL spectra under pressures of P = 0.27, 0.93, 2.12, 3.45, and 4.51 GPa. PL peaks A and T are indicated. (c) Photon energy of PL peak A as a function of the pressure. The data can be linearly fitted with a slope of 20 ± 1 meV/GPa. The energy position of peak A is represented by the open dark cyan square when the pressure releases.

monolayer MoS_2, the principal PL peak labeled A at 1.82 eV is assigned to a direct K−K interband transition between the conduction band and the upper lying valence band at the K point in the Brillouin zone (Figure 2b). The PL peak shoulder labeled B at approximately 2 eV is assigned to the direct K−K interband transition between the conduction band and the lower lying valence band. As the number of layers increases from 1 to 3, the PL intensity of peak B shows a relatively increased weight compared with that of peak A. For bilayer MoS_2, in addition to the PL peaks A and B, a PL peak labeled I at approximately 1.51 eV appears due to the indirect interband transition between the K valley of the conduction band and the Γ hill of the valence band (Figure 2c). Here, we tentatively assign the CBM of bilayer MoS_2 to the K point and will discuss this assignment in detail below. For trilayer MoS_2, the PL peak I shifts to a lower energy position, while the energies of the PL peaks A and B related to the K−K interband transition undergo no clear shift. It is known that the conduction band valley and the valence band hill at the K point are primarily constituted by d orbital wave functions that are localized around the Mo atoms. They have minimal interlayer coupling, and their energies depend insensitively on the number of the MoS_2 layer because Mo atoms are in the middle of the sandwich structure. By contrast, the valence hill at the Γ point is described by a wave function of S atoms with a p orbital character and extends beyond the plane formed by the MoS_2 sandwich, which exhibits strong interlayer coupling, and its energy is easily tuned through interlayer spacing.[1,24,28]

Figure 3a maps the PL intensity as a function of hydrostatic pressure from 0.27 to 4.87 GPa for the monolayer MoS_2 sample, whose microscopic image is displayed in the right inset. The data acquisition time for PL measurements is 4 s. The PL intensities as a function of photon energy for the pressures of 0.27, 0.93, 2.12, 3.45, and 4.51 GPa are shown in Figure 3b, with background signal having been subtracted (see Supporting Information for detail). As shown, all PL peaks, including peak A and peak T at the low energy tail, show blue shifts as the pressure increases. Here, PL peak T may be related to unintentional doping and shallow traps.[8,45] To obtain the energy position of peak A at higher pressures, the PL curves are fitted using two Gaussian functions (see Supporting Information). The energy evolution of PL peak A as a function of pressure is summarized in Figure 3c and shows a good linear increase at a rate of 20 ± 1 meV/GPa. After the pressure releases, PL peak A returns to its original energy position, represented by an open dark cyan square (Figure 3c) that indicates good optical quality of the sample under pressure. We also noticed that the emission intensity of PL peak A exhibits a significant decrease with increasing pressure. This result might be related to the strain-induced approaching the crossover point of the direct-to-indirect transition[36] and/or the pressure-induced increase of defects. However, to clarify it, more work is required.

Figure 4a maps the PL intensity as a function of hydrostatic pressure from 0.36 to 2.34 GPa for the bilayer MoS_2 sample, whose microscopic image is displayed in the right inset. The data acquisition time for PL measurements is 7 s. The PL intensities as a

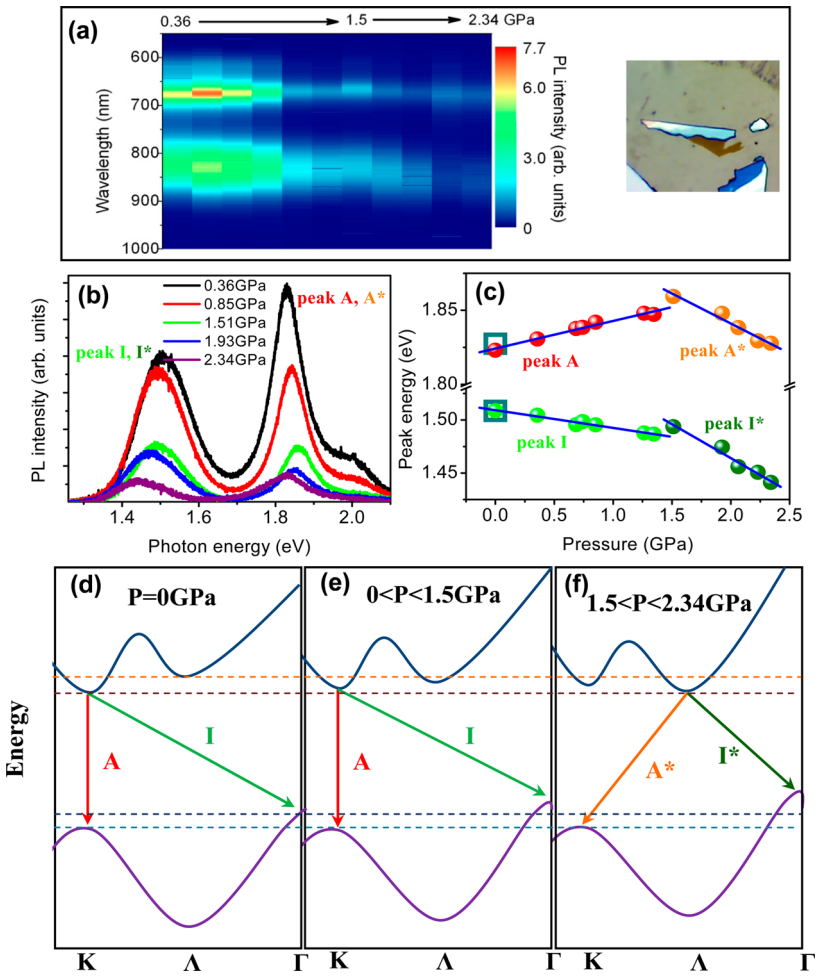

Figure 4. (a) PL intensity mapping as a function of wavelength as hydrostatic pressure increases from 0.36 to 2.34 GPa for the bilayer MoS_2 sample, whose microscopic image is shown in the right inset. A 4:1 methanol−ethanol pressure-transmitting medium is used. (b) PL spectra of the bilayer MoS_2 sample under pressures of 0.36, 0.85, 1.51, 1.93, and 2.34 GPa. PL peaks A and I are identified. (c) Photon energies of the PL peaks A, A*, I, and I* as a function of pressure are shown by red, orange, green, and olive solid circles, respectively. The data are linearly fitted, as shown by the blue lines, and the slopes of 19 ± 2, −40 ± 4, −17 ± 2, and −64 ± 6 meV/GPa are obtained for the PL peaks A, A*, I, and I*, respectively. The energy positions of peaks A and I are represented by the open dark cyan squares when the pressure releases. (d−f) Schematic representations of the band structure for bilayer MoS_2 when $P = 0$ GPa, $0 < P < 1.5$ GPa, and $1.5 < P < 2.34$ GPa. The K, Λ, and Γ points and interband transitions (A, A*, I, and I*) are identified. Four dashed lines are used to guide the eye to the shift of related energy bands.

function of photon energy for the pressures of 0.36, 0.85, 1.51, 1.93, and 2.34 GPa are shown in Figure 4b, with background signal having been subtracted (see Supporting Information for detail). In contrast to monolayer MoS_2, both the direct interband transition of peak A and indirect interband transition of peak I of bilayer MoS_2 exhibit considerably more complex evolutions of peak energy (see Figure 4c). As Figure 4c shows, a clearly pressure-induced changeover of optical gap occurs at approximately 1.5 GPa. Consequently, interband transitions of peaks A and I are changed to the labels A* and I*, respectively, when the pressure exceeds 1.5 GPa. For $0 < P < 1.5$ GPa, PL peak A shows a blue shift at a rate of 19 ± 2 meV/GPa. However, when $1.5 < P < 2.34$ GPa, PL peak A* shows a red shift at a rate of −40 ± 4 meV/GPa. For PL peak I, and when $0 < P < 1.5$ GPa, the peak shows a red shift at a rate of −17 ± 2 meV/GPa; when $1.5 < P < 2.34$ GPa, PL peak I* undergoes a more rapid red shift at a rate of −64 ± 6 meV/GPa. Again, after the pressure releases, both PL peaks A (A*) and I (I*) return to their original positions, represented by the open dark cyan squares (Figure 4c).

It is noteworthy that increasing the MoS_2 sandwich layer number nearly does not affect the direct band gap at the K point, which is insensitive to the van der Waals force between sandwiched layers.[1,24,28] Additionally, theoretical calculations show that the direct K−K interband transition of bilayer MoS_2 is considerably less susceptible to change in the out-of-plane lattice constant c induced by the compressive strain, yet increases significantly under increasing compressive in-plane strain due to the change in the in-plane lattice constant a.[30,33,40,49] Hence, the hydrostatic pressure dependence of the PL peaks A (related to direct K−K interband transition) of monolayer and bilayer MoS_2 should be consistent. Indeed, the PL peaks A of

both monolayer and bilayer MoS_2 show blue shifts with approximately identical pressure coefficients of 20 (Figure 3c) and 19 meV/GPa (Figure 4c), respectively, when the pressure is less than 1.5 GPa. This result agrees with the theoretical calculation for the upward shift of the K valley of the conduction band under a compressive strain.[28,30,40] When the applied pressure is greater than 1.5 GPa, for monolayer MoS_2, the PL peak A continues to blue shift. However, for bilayer MoS_2, a blue−red shift changeover is observed, indicating that the Λ valley becomes the CBM because the compressive strain induces a downward shift of Λ the valley, as theoretically predicted.[30,33,40] In place of peak A, PL peak A* related to the indirect Λ−K interband transition becomes the dominant peak. We believe that under zero strain, the K valley forms the CBM of bilayer MoS_2 and is actually lower than the Λ valley, similar to the case of monolayer MoS_2. Otherwise, the changeover from the direct K−K to the indirect Λ−K interband transition would not occur. In monolayer MoS_2, no changeover is observed until approximately 4.87 GPa, thereby indicating that the energy difference between the K and the Λ valleys should be much larger than that in bilayer MoS_2. Based on the positive and negative pressure coefficients of 19 ± 2 meV/GPa and -40 ± 4 meV/GPa for the K−K and the Λ−K interband transitions, respectively, as well as the changeover point of pressure at 1.5 GPa, it is deduced that the energy difference between the K and the Λ valleys ($\Delta E_{K\Lambda}$) in bilayer MoS_2 is approximately 89 ± 9 meV under zero strain, that is, $\Delta E_{K\Lambda} = (19 + 40)$ meV/GPa $\times$ 1.5 GPa. This energy difference is consistent with the value of 100 meV predicted by the density function theory (DFT) calculation[40] and other theoretical calculations.[18,26] As is known, the exciton binding energy in two-dimensional materials can be expressed as $E_b = 54.4\ \mu_{ex}/m_0\varepsilon^2$, where $\mu_{ex} = m_e m_h/(m_e + m_h)$ is the exciton effective mass; m_e and m_h are electron and hole effective masses, respectively; m_0 is the electron mass; and ε is the relative dielectric constant.[46] According to theoretical calculations,[24,30,34,36] m_e at the K and the Λ points, m_h at the K point, and ε for both monolayer and bilayer MoS_2 change little when the applied strain is less than approximately 1%. Hence, the exciton binding energies related to the K−K and the Λ−K interband transitions are insensitive to the applied strain. The measured pressure dependence of the optical gap may thus be mainly related to the changes in the electronic band structure. This conclusion is supported by the consistency between the DFT calculation and the experimental result of $\Delta E_{K\Lambda}$ of bilayer MoS_2 due to the reported result that the m_e values at the K and the Λ points are notably similar to each other under zero strain, namely, 0.542 and 0.579, respectively.[18] Here, we are aware that in monolayer and bilayer MoS_2, the exciton binding energies may be somehow modified by the applied strain, which should thus be considered for more precisely calculating the changeover of CBM from the K point to the Λ point.

Moreover, for bilayer MoS_2, PL peak I is related to the indirect K−Γ interband transition under zero strain and becomes PL peak I*, which is related to the Λ−Γ interband transition when $1.5 < P < 2.34$ GPa because, in this case, the CBM is located at the Λ point. For $0 < P < 1.5$ GPa, the PL peak I related to the K−Γ transition shows a red shift at a rate of -17 ± 2 meV/GPa. Such a negative rate reflects that the upward shift of the Γ hill occurs more quickly than does the upward shift of the K valley. This effect is attributed mainly to the change in the lattice constant c induced by compressive strain along the out-of-plane direction because the c-axis is more susceptible compared with the a-axis under hydrostatic pressure.[47,48] When $1.5 < P < 2.34$ GPa, the PL peak I* related to the Λ−Γ transition is expected to shift at a rate of -76 ± 8 meV/GPa, considering the relative shift of the Λ valley and the Γ hill that is schematically shown in Figure 4f, and based on the blue shift of the K−K transition at a rate of 19 ± 2 meV/GPa and the red shift of the Λ−K and the K−Γ transitions at rates of -40 ± 4 and -17 ± 2 meV/GPa, respectively. The value of -76 ± 8 meV/GPa is close to the observed Λ−Γ transition rate of 64 ± 6 meV/GPa. The schematic diagrams of the evolution of the band structure at the K, the Λ, and the Γ points, as well as of the related interband transitions (A, A*, I, and I*) under pressure for bilayer MoS_2 when $P = 0$ GPa, $0 < P < 1.5$ GPa, and $1.5 < P < 2.34$ GPa are shown in Figure 4d−f. The band structure shown in Figure 4f is similar to the calculated result for bulk MoS_2.[1,2]

For monolayer MoS_2, a tensile strain could induce the direct K−K to the indirect K−Γ interband transition.[18,36] In addition, a changeover between the direct K−K to the indirect Λ−K interband transition has been predicted when a biaxial compressive strain as large as 1.3%[18] or approximately 2%[28] is applied to the in-plane direction. It has also been experimentally reported that the pressure rate of the in-plane lattice constant a of bulk MoS_2 is approximately 0.24%/GPa when the hydrostatic pressure is less than 5 GPa.[47,48] In our study, the maximum hydrostatic pressure applied by the DAC device is 4.87 GPa, corresponding to an in-plane lattice constant reduction Δa of approximately 1.2%, which is slightly below the value of 1.3% for the occurrence of the predicted direct-to-indirect changeover. Moreover, the change in the direct K−K transition energy has been theoretically calculated to be approximately 92 meV per a 1% change in the in-plane lattice constant a.[28] On the basis of these data, we can deduce that the pressure coefficient of the K−K interband transition of monolayer MoS_2 will be approximately 22 meV/GPa, which agrees well with the experimental result of 20 meV/GPa obtained in our study. Furthermore, we would like to note that these discussions are

based on the assumption that few-layer and bulk MoS_2 are expected to have similar values of hydrostatic pressure rates of the in-plane lattice constant *a*. This assumption is reasonable due to recent research that indicates that the thermal expansion coefficients for few-layer and bulk MoS_2 are comparable.[40,49]

CONCLUSIONS

We have shown that both direct and indirect interband transitions of monolayer and bilayer MoS_2 can be efficiently tuned using hydrostatic pressure. The PL peak A undergoes a blue shift at a rate of approximately 20 meV/GPa for both monolayer and bilayer MoS_2, when $0 < P < 1.5$ GPa. The pressure-induced change-over point from a direct interband K−K to an indirect interband Λ−K transition is observed at approximately 1.5 GPa for bilayer MoS_2. The observed red shift rates are relatively higher for indirect interband transitions, such as −40 meV/GPa for the Λ−K transition and −64 meV/GPa for the Λ−Γ transition when $1.5 < P < 2.34$ GPa. It is demonstrated that the CBM of bilayer MoS_2 occurs at the K point, while the Λ valley in the conduction band is approximately 89 ± 9 meV higher than the K valley under zero strain.

METHODS

Sample Fabrication. The monolayer and few-layer MoS_2 samples measuring a few micrometers were prepared by micromechanical exfoliation of a natural bulk MoS_2 (SPI Supplies) on a thinned SiO_2/Si substrate. Regions of one-, two-, and three-layer MoS_2 were identified by their optical contrast with an optical microscopy. The contrasts were confirmed using PL measurements.

Micro-PL Measurements under Pressure. Micro-PL measurements were obtained at room temperature using an optical confocal microscopy setup. A continuous wave solid-state laser beam with a wavelength of 454 nm and an average power of approximately 2 mW was focused on the sample in the DAC device using a long focal length objective (20×, NA 0.35). The emitted PL was collected by the same objective; then, the PL was focused on a pinhole to suppress background emission. The PL was analyzed using a 0.5 m monochromator equipped with a Peltier-cooled silicon charge-coupled device. The pressure-dependent PL measurements were obtained using a DAC device. A mixture of methanol and ethanol at a ratio of 4:1 was used as the pressure-transmitting medium. The pressure was determined based on the shift of the R1 fluorescence line of ruby in the chamber.

Background Subtraction Method for PL Measurements. For hydrostatic pressure-dependent PL measurements, the background signals from the diamond and the pressure-transmitting medium must be subtracted from the measured raw data. To weaken the influence of the background emission on the PL peak, the measured sample was kept close to the culet face of the bottom diamond anvil. Considering the different focusing positions of the diamond anvil and the sample, the background emission from the diamond can be spatially filtered using a 100 μm pinhole with the confocal microscopy configuration.

Conflict of Interest: The authors declare no competing financial interest.

Acknowledgment. We acknowledge support from the National Key Basic Research Program of China (Grant Nos. 2013CB922304 and 2013CB933304), the National Natural Science Foundation of China (Grant Nos. 11204297 and 11374295), the Strategic Priority Research Program (B) of the Chinese Academy of Sciences (Grant No. XDB01010200), and the Tsinghua National Laboratory for Information Science and Technology (TNList) Cross-discipline Foundation.

Supporting Information Available: Optical confocal microscopy setup, the DAC device and sample processing, background signal subtraction method for the PL measurements in the DAC device, and the Gaussian fitting of the PL peaks A and T. This material is available free of charge *via* the Internet at http://pubs.acs.org.

REFERENCES AND NOTES

1. Mak, K. F.; Lee, C.; Hone, J.; Shan, J.; Heinz, T. Atomically Thin MoS_2: A New Direct-Gap Semiconductor. *Phys. Rev. Lett.* **2010**, *105*, 136805.
2. Splendiani, A.; Sun, L.; Zhang, Y.; Li, T.; Kim, J.; Chim, C.-Y.; Galli, G.; Wang, F. Emerging Photoluminescence in Monolayer MoS_2. *Nano Lett.* **2010**, *10*, 1271–1275.
3. Radisavljevic, B.; Radenovic, A.; Brivio, J.; Giacometti, V.; Kis, A. Single-Layer MoS_2 Transistors. *Nat. Nanotechnol.* **2011**, *6*, 147–150.
4. Lin, M.-W.; Liu, L.; Lan, Q.; Tan, X.; Dhindsa, K. S.; Zeng, P.; Naik, V. M.; Cheng, M. M.-C.; Zhou, Z. Mobility Enhancement and Highly Efficient Gating of Monolayer MoS_2 Transistors with Polymer Electrolyte. *J. Phys. D: Appl. Phys.* **2012**, *45*, 345102.
5. Yin, Z.; Li, H.; Li, H.; Jiang, L.; Shi, Y.; Sun, Y.; Lu, G. Single-Layer MoS_2 Phototransistors. *ACS Nano* **2012**, *6*, 74–80.
6. Lopez-Sanchez, O.; Lembke, D.; Kayci, M.; Radenovic, A.; Kis, A. Ultrasensitive Photodetectors Based on Monolayer MoS_2. *Nat. Nanotechnol.* **2013**, *8*, 497–501.
7. Sundaram, R. S.; Engel, M.; Lombardo, A.; Krupke, R.; Ferrari, A. C.; Avouris, P.; Steiner, M. Electroluminescence in Single Layer MoS_2. *Nano Lett.* **2013**, *13*, 1416–1421.
8. Mak, K. F.; He, K. L.; Shan, J.; Heinz, T. F. Control of Valley Polarization in Monolayer MoS_2 by Optical Helicity. *Nat. Nanotechnol.* **2012**, *7*, 494–498.
9. Mak, K. F.; He, K. L.; Lee, C.; Lee, G. H.; Hone, J.; Heinz, T. F.; Shan, J. Tightly Bound Trions in Monolayer MoS_2. *Nat. Mater.* **2013**, *12*, 207–211.
10. Zeng, H. L.; Dai, J. F.; Yao, W.; Xiao, D.; Cui, X. D. Valley Polarization in MoS_2 Monolayers by Optical Pumping. *Nat. Nanotechnol.* **2012**, *7*, 490–493.
11. Jones, A. M.; Yu, H. Y.; Ghimire, N.; Wu, S. F.; Aivazian, G.; Ross, J. S.; Zhao, B.; Yan, J. Q.; Mandrus, D.; Xiao, D.; *et al.* Optical Generation of Excitonic Valley Coherence in Monolayer WSe_2. *Nat. Nanotechnol.* **2013**, *8*, 634–638.
12. Cao, T.; Wang, G.; Han, W.; Ye, H.; Zhu, C.; Shi, J.; Niu, Q.; Tan, P.; Wang, E.; Liu, B.; *et al.* Valley-Selective Circular Dichroism of Monolayer Molybdenum Disulphide. *Nat. Commun.* **2012**, *3*, 887.
13. Li, T. Ideal Strength and Phonon Instability in Single-Layer MoS_2. *Phys. Rev. B* **2012**, *85*, 235407.
14. Johari, P.; Shenoy, V. B. Tuning the Electronic Properties of Semiconducting Transition Metal Dichalcogenides by Applying Mechanical Strains. *ACS Nano* **2012**, *6*, 5449–5456.
15. Scalise, E.; Houssa, M.; Pourtois, G.; Afanas'ev, V.; Stesmans, A. Strain-Induced Semiconductor to Metal Transition in the Two-Dimensional Honeycomb Structure of MoS_2. *Nano Res.* **2011**, *5*, 43–48.
16. Ghorbani-Asl, M.; Borini, S.; Kuc, A.; Heine, T. Strain-Dependent Modulation of Conductivity in Single-Layer Transition-Metal Dichalcogenides. *Phys. Rev. B* **2013**, *87*, 235434.
17. Feng, J.; Qian, X.; Huang, C.-W.; Li, J. Strain-Engineered Artificial Atom as a Broad-Spectrum Solar Energy Funnel. *Nat. Photonics* **2012**, *6*, 866–872.
18. Yun, W. S.; Han, S. W.; Hong, S. C.; Kim, I. G.; Lee, J. D. Thickness and Strain Effects on Electronic Structures of Transition Metal Dichalcogenides: 2H-MX_2 Semiconductors (M = Mo, W; X = S, Se, Te). *Phys. Rev. B* **2012**, *85*, 033305.

19. Lu, P.; Wu, X.; Guo, W.; Zeng, X. C. Strain-Dependent Electronic and Magnetic Properties of MoS_2 Monolayer, Bilayer, Nanoribbons and Nanotubes. *Phys. Chem. Chem. Phys.* **2012**, *14*, 13035–13040.
20. Kou, L.; Tang, C.; Zhang, Y.; Heine, T.; Chen, C.; Frauenheim, T. Tuning Magnetism and Electronic Phase Transitions by Strain and Electric Field in Zigzag MoS_2 Nanoribbons. *J. Phys. Chem. Lett.* **2012**, *3*, 2934–2941.
21. Peelaers, H.; Van de Walle, C. G. Effects of Strain on Band Structure and Effective Masses in MoS_2. *Phys. Rev. B* **2012**, *86*, 241401(R).
22. Horzum, S.; Sahin, H.; Cahangirov, S.; Cudazzo, P.; Rubio, A.; Serin, T.; Peeters, F. M. Phonon Softening and Direct to Indirect Band Gap Crossover in Strained Single-Layer $MoSe_2$. *Phys. Rev. B* **2013**, *87*, 125415.
23. Kuc, A.; Zibouche, N.; Heine, T. Influence of Quantum Confinement on the Electronic Structure of the Transition Metal Sulfide TS_2. *Phys. Rev. B* **2011**, *83*, 245213.
24. Shi, H. L.; Pan, H.; Zhang, Y. W.; Yakobson, B. I. Quasiparticle Band Structures and Optical Properties of Strained Monolayer MoS_2 and WS_2. *Phys. Rev. B* **2013**, *87*, 155304.
25. Ramasubramaniam, A.; Naveh, D.; Towe, E. Tunable Band Gaps in Bilayer Transition-Metal Dichalcogenides. *Phys. Rev. B* **2011**, *84*, 205325.
26. Cheiwchanchamnangij, T.; Lambrecht, W. R. L. Quasiparticle Band Structure Calculation of Monolayer, Bilayer, and Bulk MoS_2. *Phys. Rev. B* **2012**, *85*, 205302.
27. Komsa, H. P.; Krasheninnikov, A. V. Effects of Confinement and Environment on the Electronic Structure and Exciton Binding Energy of MoS_2 From First Principles. *Phys. Rev. B* **2012**, *86*, 241201.
28. Chang, C. H.; Fan, X. F.; Lin, S. H.; Kuo, J. L. Orbital Analysis of Electronic Structure and Phonon Dispersion in MoS_2, $MoSe_2$, WS_2, and WSe_2 Monolayers under Strain. *Phys. Rev. B* **2013**, *88*, 195420.
29. Molina-Śanchez, A.; Sangalli, D.; Hummer, K.; Marini, A.; Wirtz, L. Effect of Spin-Orbit Interaction on the Optical Spectra of Single-Layer, Double-layer, and Bulk MoS_2. *Phys. Rev. B* **2013**, *88*, 045412.
30. Dong, L.; Dongare, A. M.; Namburu, R. R.; O'Regan, T. P.; Dubey, M. Theoretical Study on Strain Induced Variations in Electronic Properties of 2H-MoS_2 Bilayer Sheets. *Appl. Phys. Lett.* **2014**, *104*, 053107.
31. Castellanos-Gomez, A.; Roldán, R.; Cappelluti, E.; Buscema, M.; Guinea, F.; van der Zant, H. S. J.; Steele, G. A. Local Strain Engineering in Atomically Thin MoS_2. *Nano Lett.* **2013**, *13*, 5361–5366.
32. Bhattacharyya, S.; Singh, A. K. Semiconductor-Metal Transition in Semiconducting Bilayer Sheets of Transition-Metal Dichalcogenides. *Phys. Rev. B* **2012**, *86*, 075454.
33. Kumar, A.; Ahluwalia, P. K. Semiconductor to Metal Transition in Bilayer Transition Metals Dichalcogenides MX_2 (M = Mo, W; X = S, Se, Te). *Modell. Simul. Mater. Sci. Eng.* **2013**, *21*, 065015.
34. Scalise, E.; Houssa, M.; Pourtois, G.; Afanaśev, V. V.; Stesmans, A. First-Principles Study of Strained 2D MoS_2. *Physica E* **2014**, *56*, 416–421.
35. He, K.; Poole, C.; Mak, K. F.; Shan, J. Experimental Demonstration of Continuous Electronic Structure Tuning *via* Strain in Atomically Thin MoS_2. *Nano Lett.* **2013**, *13*, 2931–2936.
36. Conley, H.; Wang, B.; Ziegler, J.; Haglund, R. F.; Pantelides, S. T.; Bolotin, K. I. Bandgap Engineering of Strained Monolayer and Bilayer MoS_2. *Nano Lett.* **2013**, *13*, 3626–3630.
37. Zhu, C. R.; Wang, G.; Liu, B. L.; Marie, X.; Qiao, X. F.; Zhang, X.; Wu, X. X.; Fan, H.; Tan, P. H.; Amand, T.; *et al.* Strain Tuning of Optical Emission Energy and Polarization in Monolayer and Bilayer MoS_2. *Phys. Rev. B* **2013**, *88*, 121301(R).
38. Hui, Y. Y.; Liu, X.; Jie, W.; Chan, N. Y.; Hao, J.; Hsu, Y.-T.; Li, L.-J.; Guo, W.; Lau, S. P. Exceptional Tunability of Band Energy in a Compressively Strained Trilayer MoS_2 Sheet. *ACS Nano* **2013**, *7*, 7126–7131.
39. Nayak, A. P.; Bhattacharyya, S.; Zhu, J.; Liu, J.; Wu, X.; Pandey, T.; Jin, C.; Singh, A. K.; Akinwande, D.; Lin, J.-F. Pressure-Induced Semiconducting to Metallic Transition in Multilayered Molybdenum Disulphide. *Nat. Commun.* **2014**, *5*, 3731.
40. Zhao, W. J.; Ribeiro, R. M.; Toh, M. L.; Carvalho, A.; Kloc, C.; Castro Neto, A. H.; Eda, G. Origin of Indirect Optical Transitions in Few-Layer MoS_2, WS_2, and WSe_2. *Nano Lett.* **2013**, *13*, 5627–5634.
41. Bassett, W. A. Diamond Anvil Cell, 50th Birthday. *High Press. Res.* **2008**, *29*, 163.
42. Lyapin, S. G.; Itskevich, I. E.; Trojan, I. A.; Klipstein, P. C.; Polimeni, A.; Eaves, L.; Main, P. C.; Henini, M. Pressure-Induced G-X Crossover in Self-Assembled In(Ga)As/GaAs Quantum Dots. *Phys. Status Solidi B* **1999**, *211*, 79–83.
43. Zhou, P. Y.; Dou, X. M.; Wu, X. F.; Ding, K.; Li, M. F.; Ni, H. Q.; Niu, Z. C.; Jiang, D. S.; Sun, B. Q. Single-Photon Property Characterization of 1.3 μm Emissions from InAs/GaAs Quantum Dots Using Silicon Avalanche Photodiodes. *Sci. Rep.* **2014**, *4*, 3633.
44. Nicolle, J.; Machon, D.; Poncharal, P.; Pierre-Louis, O.; San-Miguel, A. Pressure-Mediated Doping in Graphene. *Nano Lett.* **2011**, *11*, 3564–3568.
45. Plechinger, G.; Schrettenbrunner, F.-X.; Eroms, J.; Weiss, D.; Schüller, C.; Korn, T. Low-Temperature Photoluminescence of Oxide-Covered Single-Layer MoS_2. *Phys. Status Solidi RRL* **2012**, *6*, 126–128.
46. Ramasubramaniam, A. Large Excitonic Effects in Monolayers of Molybdenum and Tungsten Dichalcogenides. *Phys. Rev. B* **2012**, *86*, 115409.
47. Aksoy, R.; Ma, Y. Z.; Selvi, E.; Chyu, M. C.; Ertas, A.; White, A. X-ray Diffraction Study of Molybdenum Disulfide to 38.8 GPa. *J. Phys. Chem. Solids* **2006**, *67*, 1914–1917.
48. Bandaru, N.; Kumar, R. S.; Sneed, D.; Tschauner, O.; Baker, J.; Antonio, D.; Luo, S. N.; Hartmann, T.; Zhao, Y. S.; Venkat, R. Effect of Pressure and Temperature on Structural Stability of MoS_2. *J. Phys. Chem. C* **2014**, *118*, 3230–3235.
49. Tongay, S.; Zhou, J.; Ataca, C.; Lo, K.; Matthews, T. S.; Li, J.; Grossman, J. C.; Wu, J. Thermally Driven Crossover from Indirect toward Direct Bandgap in 2D Semiconductors: $MoSe_2$ *versus* MoS_2. *Nano Lett.* **2012**, *12*, 5576–5580.